


## PAPER

[View Article Online](#)  
[View Journal](#) | [View Issue](#)Cite this: *RSC Sustainability*, 2024, 2, 686**Adsorptive decolorization of dyes in aqueous solution using magnetic sweet potato (*Ipomoea batatas* L.) peel waste**Paul N. Diagboya, \* Alexander Odagwe, Henry H. Oyem, Chiadika Omoruyi and Emmanuel Osabohien

Valorizing domestic biomass waste for contaminated water treatment may be an effective way to achieve the sustainable development goal of attaining clean water for all. Hence, sweet potato peel (SPP) waste was valorized by magnetizing the pretreated SPP adsorbent to prepare the magnetized adsorbent (MSP) which was employed for methylene blue (MB) sorption. The MSP exhibited enhanced cation exchange capacity (11%) and MB sorption greater than 100% of either of the starting pristine materials. Sorption equilibrium was fast (20 min), and the adsorbent was effective over a wide pH (3–9) and temperature range (15–35 °C). The observed sorption capacity of the MSP for MB was 14.3 mg g<sup>-1</sup> and this is better than those of most biomass-based adsorbents reported in the literature. The composite exhibited good reusability with ≈70% efficiency after 5 cycles. The MB sorption mechanism was a rather complex process involving electrostatic interaction, multi-layer adsorption, and pore-filling. Notwithstanding the enhanced sorption capacity, the ease of magnetic separation of the MSP adsorbent from water post-adsorption, its stability, and reusability are the major merits of this adsorbent. These facts make the MSP composite an appealing cost-effective choice for treating MB-contaminated water.

Received 6th November 2023  
Accepted 18th January 2024

DOI: 10.1039/d3su00410d

[rsc.li/rscsus](https://rsc.li/rscsus)**Sustainability spotlight**

Contaminated water is a serious concern because it has been linked to several diseases and health challenges. Achieving the UN sustainable development goal of clean water for all is quite a difficult challenge for low-income countries due to intractable pollution sources, lack of technical know-how, and cost of water treatment; water pollution is unprecedented and increasing. Thus, it is vital to develop easily accessible, cheap, and easy-to-use technologies for water treatment, especially for small scale industries. Hence, we valorized common domestic waste by magnetization and employed it for dye-contaminated water treatment in order to achieve the sustainable development goal of attaining clean water for all. Preparation and use (and multiple reuses) are easy and may be achieved by inexperienced users.

**1 Introduction**

Industrial contamination of potable water sources is an issue of serious concern due to the persistence and toxicity of most water contaminants.<sup>1</sup> The magnitude of this challenge is unprecedented due to several recent industrial inputs but has been compounded by other sources such as the emerging contaminants from municipalities and pesticides from agriculture.<sup>2,3</sup> It is estimated that approximately 60% of the global population either lack adequate sanitary facilities or have no access to any type of proper water treatment facility.<sup>4</sup> The majority of these water-stressed populations live in low-income or developing countries where advanced water treatment techniques are expensive and unavailable. Hence, the need for low-cost treatment techniques cannot be underestimated.

Common water contaminants include dyes which are used as coloring agents, and found in effluents released from leather, cosmetics, paper, and textile industries.<sup>5</sup> Dyes are toxic to biota, and some are known carcinogens.<sup>5,6</sup> In addition to affecting the quality of water, the toxicity of dyes makes it important to eliminate them from water. A typical example is methylene blue (MB) which was used in this study as a model dye contaminant. It is a cationic dye of utmost concern due to the presence of a similar cationic moiety as found in several commonly used reactive dyes. The presence of the benzene ring structure, as well as the N and S atoms makes it difficult to degrade and toxic. It has been reported to be mutagenic, causing serotonin syndrome which results in breakdown of red blood cells, and irritation of the skin and the eyes.<sup>7</sup> Dyes are the mainstay of the tie-dye industry in sub-Saharan Africa, and pollution of water bodies is common in the vicinities of this type of industry. Advanced water treatment technologies such as ion exchange, electrochemical treatment, chemical precipitation, membrane

*Environmental Fate of Chemicals and Remediation (EnFaCRe) Laboratory, University of Delta, Agbor, Nigeria. E-mail: pauldn2@yahoo.com*



technology, and reverse osmosis are too expensive to be applied in small-scale industries, especially in low-income or developing countries.<sup>2,8</sup> Compared to these techniques, adsorption-based methods are very cheap, easy to apply, environmentally friendly, and present the least techno-economic challenges.<sup>8–13</sup> Different locally available materials, including wastes and biomass, may be used,<sup>4,8,14</sup> and their surface chemistry can be tuned for enhanced contaminant sorption,<sup>3,4,8,15</sup> while the used adsorbents may be regenerated and reused.

Some of the studied low-cost adsorbents for the adsorption of aqueous dyes and other water contaminants include nonliving moss,<sup>14,16</sup> *Moringa oleifera* seed waste,<sup>3,17</sup> sweet potato peel,<sup>18</sup> banana peel,<sup>19</sup> *Nauclea diderrichii* seed biomass,<sup>20</sup> yam peel,<sup>21</sup> and tamarind fruit shell.<sup>22</sup> One major advantage of employing low-cost or agricultural materials and unwanted domestic wastes is that it eliminates or reduces the undesirable effects of these wastes on the environment. For instance, yam (*Dioscorea* spp) and sweet potato (*Ipomoea batatas* L.) are common staples in sub-Saharan Africa, and large amounts of waste (millions of tonnes) are generated from their peels.<sup>18,21</sup> The bulk of these wastes may not be used in other applications, and constitute a nuisance in the environment. Thus, using these wastes as biosorbents for water treatment is cheap and would improve the aesthetics of the environment. In this regard, sweet potato peel (a common sub-Saharan waste) was employed as an adsorbent in this study.

Sweet potato waste-based materials have been employed as adsorbents in some studies.<sup>18,23,24</sup> These sweet potato-based adsorbents have shown promising results, but a major shortcoming of these studies is the difficulty in separating the adsorbents post-adsorption. The traditional centrifugation and filtration-based techniques are expensive and cumbersome, and the equipment used to perform these techniques becomes considerably huge when handling large volumes of effluent water. Magnetization of low-cost adsorbents presents a potentially cost-effective and less cumbersome method to separate adsorbents post-adsorption, as well as increase adsorbent efficiency.<sup>4,6,25,26</sup> Hence, the objective of this study was to magnetize the sweet potato peel waste adsorbent, use it for the adsorption of MB from aqueous solution, and easily separate the magnetized adsorbent from water post-adsorption under the influence of a magnetic field. The adsorption data will be described using various adsorption models.

## 2 Materials and methods

### 2.1 Biomass treatment and preparation of magnetic biomass

Sweet potato (*Ipomoea batatas* L.) was obtained from a local Nigerian market, and washed with tap water before peeling the bark. The peeled bark (waste) was oven-dried at 110 °C until constant weight to remove water and pulverized to fineness. It was then soaked in ethyl acetate overnight to remove oils and fats. The cake obtained was oven-dried at 110 °C to remove all traces of water, cooled, sieved through a 230 mesh size sieve, and stored in an air-tight container before the study. This was called the sweet potato peel (SPP) waste.

Analytical-grade reagents obtained from Sigma-Aldrich and deionized water were used throughout the study. Methylene blue (CAS: 61-73-4;  $C_{16}H_{18}ClN_3S$ ; MW: 319.86) stock solution of 500 mg L<sup>-1</sup> was used to prepare the working solutions employed in the study. Magnetic (Fe<sub>3</sub>O<sub>4</sub>) nano-particles were prepared using the chemical co-precipitation method<sup>4,25,26</sup> by mixing FeCl<sub>3</sub> (CAS: 7705-08-0; MW: 162.2) (3.0 mL; 1 M) and FeCl<sub>2</sub> (CAS: 7758-94-3; MW: 126.75) (1.0 mL; 2 M) solutions in a 250 mL beaker containing a magnetic stirring bar. The beaker was continuously stirred while slowly adding NaOH (2 M) solution. The addition of the NaOH base was stopped with the magnetic stirrer turned off once the initial brown iron solution turned black indicating the formation of magnetite. The ferro-fluid was allowed to settle and the supernatant was decanted while the stirrer bar was removed. The magnetic nanoparticles (MNP) were washed four times with water and ethanol interchangeably, and the particles were separated from the solution by decantation and air-dried. The magnetic nanoparticles-biomass hybrid (MSP) was prepared as above but by adding 500 mg of SPP to the MNP before washing and continuously stirring for 2 h. The mixture was then filtered, the residue air-dried and stored.

### 2.2 Adsorbent characterization

The physicochemical characterization of the pristine and magnetized adsorbent was carried out using various instruments and methods. The adsorbents' pH values were determined in deionized water and 1 M KCl, and the pH at point of zero charge (pHpzc) values were determined by the solid addition method, while the cation exchange capacity (CEC) values were determined by the sodium saturation method.<sup>27</sup> The Fourier transform infrared (FTIR) and thermo-gravimetric analysis (TGA) spectra were obtained using a FTIR spectrometer (Spectrum Two, PerkinElmer Instruments, USA), and Pyris Diamond Thermo-gravimetric analyzer (TGA 400, PerkinElmer Instruments, USA), respectively, while the scanning electron micrographs (SEM) were captured using a Zeiss Auriga Field Emission Scanning Electron Microscope (Germany), and the X-ray diffractograms were obtained using an X-ray diffractometer (XRD-7000, Shimadzu, Japan).

### 2.3 Methylene blue decolorization studies and data treatment

The SPP, MNP, and MSP were used in preliminary adsorption experiments to estimate their MB uptake capacities. This was followed by the determination of the effects of operating variables (time, pH, MB concentration, and temperature) on the uptake of aqueous MB by the MSP. Batch experiments were carried out in duplicate by adding 10 mL of aqueous MB solution (100 mg L<sup>-1</sup>) (except for the effect of MB concentration on uptake) into experimental vials containing 200 mg of the adsorbent. This mixture was equilibrated at 25 °C until equilibrium. The pH of the experimental mixture was adjusted as required during the study by adding drops of either 0.1 M HCl or NaOH solutions. The effect of time on the uptake was investigated by varying the time from 5–180 min, the effect of



pH was studied by varying the pH from 3–9, and the effect of MB concentration was studied by varying the concentration from 50–300 mg L<sup>-1</sup> with a 20 min equilibration time, while the effect of temperature was a repeat of the effect of concentration carried out at 15, 25 and 35 °C. The concentration of MB remaining in the solution after each uptake study was determined using a UV-visible spectrophotometer (PerkinElmer, USA) at the wavelength of 665 nm.

The reusability study was carried out by washing twice the MB-loaded MSP with 20 mL of ethanol:water (50 : 50%) solution on a thermostatic shaker at 200 rpm for 1 h each, and oven drying at 60 °C for 3 h. The washed MSP composite (200 mg) was then reused for MB sorption using 50 mg L<sup>-1</sup> of MB solution. This process was repeated five times.

The initial ( $C_o$ ) and final ( $C_e$ ) concentrations of aqueous MB were employed to estimate the extent of MB uptake at equilibrium using eqn (1)

$$q_e = (C_o - C_e)v/m \quad (1)$$

where  $q_e$ ,  $v$ , and  $m$  are the MB adsorbed (mg g<sup>-1</sup>), volume of the solution (mL), and mass (mg) of the MSP adsorbent used, respectively.

The rate data for MB uptake were obtained using three non-linear kinetics models: the pseudo-first-order (PFO) (eqn (2)),<sup>28</sup> pseudo-second-order (PSO) (eqn (3)),<sup>29</sup> and fractal pseudo-second-order (FPSO) (eqn (4))<sup>29</sup> kinetics models.

$$q_t = q_e(1 - e^{-k_1 t}) \quad (2)$$

$$q_t = \frac{q_e^2 k_2 t}{1 + q_e k_2 t} \quad (3)$$

$$q_t = \frac{k_f q_e^2 t^\alpha}{1 + k_f q_e t^\alpha} \quad (4)$$

The quantities  $q_e$  and  $q_t$  represent MB uptake (mg g<sup>-1</sup>) at equilibrium and time  $t$ , respectively, while the rate constants of pseudo-first and second-order, as well as the FPSO are  $k_1$  (min<sup>-1</sup>),  $k_2$  (g mg<sup>-1</sup> min<sup>-1</sup>), and  $k_f$  (L g<sup>-1</sup>), respectively.

The equilibrium data at all three temperatures were described using three non-linear adsorption isotherm models: the Langmuir (eqn (5)),<sup>30</sup> Freundlich (eqn (6)),<sup>30</sup> and Brouers–Sotolongo–fractal (eqn (7))<sup>29</sup> models, as well as the thermodynamic parameters: equilibrium constants ( $K_C$ ) (eqn (8)), entropy change ( $\Delta S^\circ$ ) (eqn (9)), enthalpy change ( $\Delta H^\circ$ ) (eqn (9)), and Gibbs free energy ( $\Delta G^\circ$ ) (eqn (10)). The  $K_C$  is the intercept of the plot of  $q_e$  vs.  $C_e$ , while the other parameters were determined from the plot of  $\ln K_C$  vs.  $1/T$  (eqn (9)). The parameters  $q_e$  and  $C_e$  are the same as above, while  $Q_{o/\max}$ ,  $b$ ,  $k_f$ ,  $n$ ,  $\alpha$ , and  $K_W$  are the maximum adsorption capacity per adsorbent unit weight, solute–surface interaction energy-related parameter, Freundlich isotherm constant, Freundlich model linearity parameter, fractional time index, and the Brouers–Sotolongo fractal constant, respectively. All model parameters were generated using OriginPro 2015 computer software.

$$q_e = \frac{Q_o b C_e}{1 + b C_e} \quad (5)$$

$$q_e = k_f C_e^n \quad (6)$$

$$Q_e = Q_{\max}(1 - (\exp(-K_W C_e^\alpha))) \quad (7)$$

$$K_C = \frac{q_e}{C_e} \quad (8)$$

$$\ln K_C = \frac{\Delta S^\circ}{R} - \frac{\Delta H^\circ}{RT} \quad (9)$$

$$\Delta G^\circ = -RT \ln K_C \quad (10)$$

### 3 Results and discussion

#### 3.1 Physicochemical characteristics of SPP, MNP, and MSP

The logic behind the magnetization process was to ease the separation of the adsorbent from water after the adsorption and, possibly, enhance the adsorption efficiency. Thus, the MNP and biomass were combined in a ratio of  $\approx 1:1$  for the adsorbent to exhibit a strong enough magnetism to be affected by an external magnetic field. To empirically establish that the magnetization process was effective and impacted the physicochemical properties, physical examination under a magnetic field showed that the adsorbent could be separated from the solution (Fig. 1a). Further comparative characterization of the pristine and composite adsorbents was carried and the results are shown in Table 1 and Fig. 1b and c. The results showed marked differences between these adsorbents. These included a higher cation exchange capacity (CEC) of over 45 and 11% for the MNP and SPP, respectively (Table 1). This higher CEC was suggestive of enhanced sorption cation efficiency in the magnetic composite,<sup>4</sup> and this was examined subsequently. The MSP composite's pH<sub>pzc</sub> value (Table 1) was slightly alkaline ( $\approx 7.5$ ) while those of the MNP (5.9) and SPP were slightly acidic (6.5). The pH<sub>pzc</sub> indicates the likely charge density on the adsorbent surface below and above the pH<sub>pzc</sub> value; above, the surface charge density is negative and the adsorbent would attract positive ions, while below the value, it is positive and the surface would attract negative ions.<sup>31</sup> In pure water, these adsorbents exhibited alkaline pH values (Table 1), while these values were slightly lower, but mainly alkaline when the pH was tested in 1 M KCl solution. Similar alkaline pH values were reported in the literature for raw biomasses.<sup>4</sup>

The FTIR spectra of all three adsorbents scanned between 4000 and 450 cm<sup>-1</sup> are presented in Fig. 1b. Characteristics biomass peaks were exhibited by the SPP spectra (Fig. 1b) and these include the hydroxyl peaks at around 3300 cm<sup>-1</sup>, and the amide peaks at 1650 cm<sup>-1</sup>, as well as the carbonyl, carboxyl, ketone, aromatic methyl groups, and alkane C–H all found between 1400 and 1000 cm<sup>-1</sup>.<sup>4,7,29</sup> Major group deformations including those of thio-esters were observed below 1000 cm<sup>-1</sup>.<sup>4,32,33</sup> The magnetic composite (MSP) exhibited these



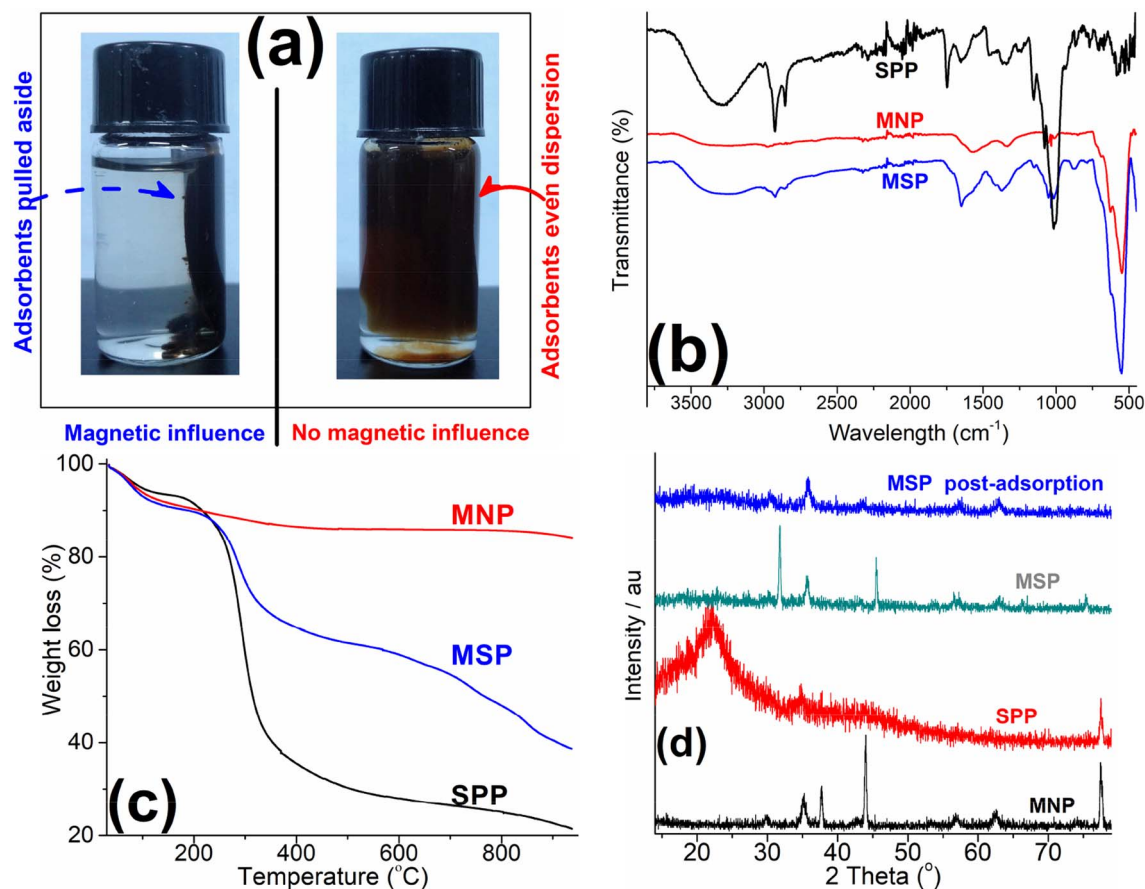


Fig. 1 (a) Adsorbent separation under the influence of a magnetic field; (b) FTIR spectra of SPP, MNP, and MSP; (c) TGA spectra of SPP, MNP, and MSP; (d) XRD diffractograms of the pristine and composite adsorbents.

Table 1 Adsorbent characterization result

Adsorbent	pH in H <sub>2</sub> O	pH in KCl	pHpzc	CEC (meq/100 g)
SPP	7.8	5.6	6.5	16.2
MNP	8.3	7.6	5.9	12.4
MSP	9.1	8.2	7.5	18.1

groups found in the SPP adsorbents in addition to the notable intense peak of the Fe–O group associated with iron oxide in MNP which was uniquely expressed at 548 cm<sup>-1</sup> (Fig. 1b).<sup>34,35</sup> This appearance of the Fe–O peak is an indication of the transference of magnetic properties to the composite adsorbent.

TGA spectra obtained for the pristine and composite adsorbents in the temperature range of 40 and 900 °C are depicted in Fig. 1c. It was observed that the MNP exhibited a high stability losing <6% mass at 900 °C. The SPP biomass on the other hand was quite labile and lost ≈78% mass at the final temperature of 900 °C. The MSP composite exhibited a stability that was in between that of the MNP and the SPP adsorbents: it lost ≈60% of its mass at the final temperature of 900 °C. The weight losses (usually ≤6) observed in the initial stage from the spectra of these adsorbents below 120 °C could be attributed to the loss of water

molecules trapped or embedded within the adsorbent mass.<sup>4,31,36</sup> The next significant weight losses (between 30 and 60% loss) were observed around 300 °C, especially for the SPP and MSP adsorbents; this was ascribed to massive volatilization of labile oxygen-containing groups as well as a breakdown of some of the less stable backbone structures of the biomass.<sup>4</sup> Subsequent weight losses could be attributed to an almost total collapse of the biomass structure.

The XRD diffractogram of the SPP, MNP and MSP composite adsorbents are shown in Fig. 1d. The SPP diffractogram exhibited typical biomass amorphous spectra showing an intense cellulose identifier peak at a 2θ angle around 22°,<sup>37,38</sup> while the MNP spectra expressed characteristic Fe<sub>3</sub>O<sub>4</sub> spinal structure peaks at 2θ values of ≈30, 36, 44, 57, 63, and 77°. <sup>37,39,40</sup> In the MSP composite spectra, the intensity of the amorphous biomass in the composite was highly oppressed while the spinal Fe<sub>3</sub>O<sub>4</sub> peaks were mostly expressed albeit with slight shifts and lowered intensities. Post-adsorption, these peaks were not altered but slightly suppressed likely due to the presence of the MB covering the Fe<sub>3</sub>O<sub>4</sub> spinal structures upon adsorption.

### 3.2 Adsorptive discoloration: rate, kinetics, and pH studies

The characterization data described above showed that the adsorbents were ultimately altered in the final composite and





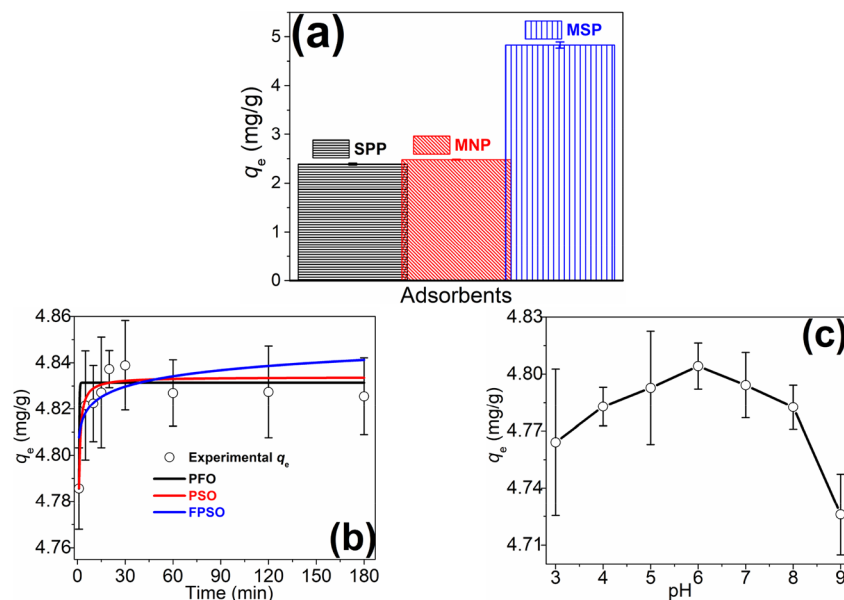


Fig. 2 (a) Comparison of preliminary MB adsorption for SPP, MNP, and MSP; (b) adsorption rate trend and kinetics modeling of MB adsorption on MSP; (c) adsorption trend at varying solution pH.

this could have an impact on the MB sorption potential of these adsorbents. Thus, a preliminary sorption experiment was carried out with the three adsorbents to prove this assertion and the results are depicted in Fig. 2a. It was observed that both the pristine biomass (SPP) and the MNP exhibited almost equal MB sorption potential. However, the MSP exhibited MB sorption which was 100% higher than either adsorbent. The higher MB sorption showed that the MSP composite was not only easier to separate from the solution post-adsorption, but the combination enhanced the MB sorption efficiency by providing more active sorption sites.

The MB sorption rate on the better-performing MSP composite was subsequently investigated and the sorption trend is detailed in Fig. 2b. It was observed that the sorption process was fast and reached equilibrium within 15 min. There was an initial increase in MB uptake within the first 10 min before equilibrium attainment when the rate of MB uptake and desorption became equal. The fast uptake process could be ascribed to the high affinity of MB to the rich vacant sorption sites available on the MSP surface.<sup>29,36</sup>

In describing the MB sorption process on the MSP, three kinetics models (PFO, PSO, and FPSO) were used to fit the experimental data with their fitting curves depicted in Fig. 2b and model parameters presented in Table 2. Assessing which model fits the data best is usually based on the closeness of the correlation coefficient ( $r^2$ ) value to unity, the lowest chi-square ( $\chi^2$ ), and sometimes the closeness of the calculated  $q_e$  value to the experimental  $q_e$ . Hence, comparing the values of all models' parameters in Table 2 showed that the PFO and PSO models could be used to explain the data because they have better model parameters: the  $r^2$  value was closer to unity ( $\geq 0.78$ ) with lower  $\chi^2$  ( $\leq 0.21$ ) values, and the calculated  $q_e$  (4.83 mg g<sup>-1</sup>) values were equal to the actual experimental  $q_e$  values. The PFO is mostly used to describe fast sorption processes that are

completed within a short time compared to the entire experiment duration;<sup>41,42</sup> this was the case for MB sorption on the MSP composite (Fig. 2b). Again, according to the fitting data, the process could also be explained by the PSO model, implying that the process was dominated by the sharing of electrons through electrostatic interactions between the sorption sites and the MB.<sup>43,44</sup> Thus, MB sorption on the MSP was a fast process dominated by electrostatic interactions.

The sorption trend at varying solution pH was also investigated and the trend is presented in Fig. 2c. This is vital because solution pH influences the extent of charge speciation for both the adsorbent and the adsorptive.<sup>7</sup> Though there was no huge difference over the entire pH region studied, the slight differences showed an increased MB sorption as pH increased from 3 to 6, and subsequently, there was a slight reduction in sorption towards pH 9. This suggests that the composite adsorbent may be employed for MB removal over a wide pH range. Adsorption

Table 2 Methylene blue discoloration kinetics model parameters

Kinetics model	Parameter	
PFO	$q_e$ (mg g <sup>-1</sup> )	4.83
	$k_1$ (min <sup>-1</sup> )	4.66
	$r^2$	0.782
	$\chi^2$	0.207
PSO	$q_e$ (mg g <sup>-1</sup> )	4.83
	$k_2$ (g mg <sup>-1</sup> min <sup>-1</sup> )	20.6
	$r^2$	0.798
	$\chi^2$	0.193
FPSO	$q_e$ (mg g <sup>-1</sup> )	7.54
	$k_f$	0.233
	$\alpha$	0.004
	$r^2$	0.143
Experimental	$\chi^2$	0.817
	$q_e$ (mg g <sup>-1</sup> )	4.83



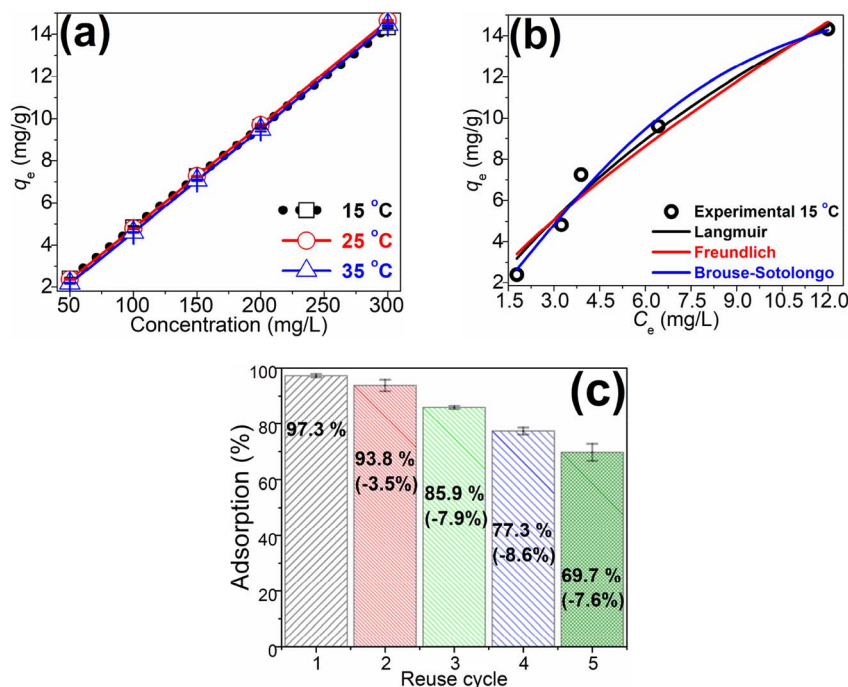


Fig. 3 (a) Adsorption trends at varying concentrations and temperatures; (b) comparison of various adsorption isotherm models at 15 °C; (c) MSP reuse graph over 5 cycles.

of contaminants over a wide pH margin could be associated with some composite as other studies have reported that composite adsorbents could be employed to adsorb contaminants over a wide pH range,<sup>29,30,45–47</sup> and this may be associated with the enhanced nature of the composite which eliminated some drawbacks of the pristine adsorbents. Thus, irrespective of the ionization state of the MB, the composite can significantly adsorb it.

### 3.3 Adsorptive discoloration dynamics

To understand the uptake dynamics, MB equilibrium sorption on the MSP adsorbent was carried out at varying MB concentrations (50–300 mg L<sup>−1</sup>) and ambient temperatures (15–35 °C).

The MB sorption trend is presented in Fig. 3a, and it shows that sorption increased linearly with rising MB concentration (within the studied concentration range). A similar trend was observed at all studied temperatures, however, no significant difference in MB sorption was observed as the temperature was varied from 15 to 35 °C. Thus, similar to the pH study, the MSP adsorbent could be employed over a wide temperature range. The enhanced MB uptake on the MSP has been attributed to the abundant sorption sites available to accommodate the adsorptive molecules as the concentration increased.<sup>1,29</sup> The increasing MB uptake even at saturation of the MSP sorption sites may be ascribed to the multi-layer adsorption of MB on already adsorbed MB on the MSP surface;<sup>29,48</sup> this could be tested by fitting

Table 3 Adsorption isotherm model parameters at varying temperatures for methylene blue

Adsorption isotherm	Parameter	MSP@15 °C	MSP@25 °C	MSP@35 °C
Langmuir model	$Q_o$ (mg g <sup>−1</sup> )	38.0	999 <sup>a</sup>	999 <sup>a</sup>
	$b$	0.05	$3.5 \times 10^{-5}$	$3.2 \times 10^{-5}$
	$r^2$	0.970	0.670	0.095
	$\chi^2$	0.63	7.36	20.23
Freundlich model	$k_F$	2.18	0.26	$8.6 \times 10^{-5}$
	$n$	0.76	2.15	5.64
	$r^2$	0.955	0.994	0.952
	$\chi^2$	0.94	0.13	1.08
Fractal Brouers–Sotolongo model	$Q_{max}$ (mg g <sup>−1</sup> )	16.0	712.2	17.2
	$K_w$	0.08	$3.5 \times 10^{-4}$	$4.8 \times 10^{-9}$
	$\alpha$	1.31	2.16	9.2
	$r^2$	0.971	0.991	0.956
Experimental	$\chi^2$	0.59	0.20	0.98
	$q_e$ (mg g <sup>−1</sup> )	14.3	14.60	14.5

<sup>a</sup> Over-estimation.



varying adsorption isotherm models to the equilibrium data. If the assumption is correct, then Freundlich-like models would fit the data.

Three adsorption isotherm models (the Langmuir, Freundlich, and fractal Brouse–Sotolongo) were fitted to the MB equilibrium data, and the model fittings at 15 °C (since there was no significant difference in the sorption data at other temperatures) are presented in Fig. 3b, while the model parameters are shown in Table 3. Assessing these models' fitness parameter ( $r^2$ ,  $\chi^2$ , and  $q_e$ ) values in Table 3, it was observed that these parameters for the Freundlich adsorption isotherm model were best with high  $r^2$  values  $\geq 0.952$  and low  $\chi^2$  values  $\leq 1.08$ . This implies that the Freundlich model fits the equilibrium data well and could be described by it. This model describes MB sorption on the heterogeneous MSP composite surfaces with a dissimilar affinity for the MB molecule, and the presence of multi-layer adsorption.

A close look at the Brouse–Sotolongo adsorption isotherm model showed that though the model over-estimated the  $q_e$  values, especially at 25 °C, the high  $r^2$  values ( $\geq 0.956$ ) and low  $\chi^2$  values ( $\leq 0.98$ ) suggest that the MB sorption on the MSP is more of a complex process. As predicted above, models that incorporate the Freundlich adsorption isotherm model would describe the MB sorption on MSP to a large extent, and hence, the good fits of the Freundlich and fractal Brouse–Sotolongo models.

Evaluating the data obtained from the kinetics and adsorption isotherm models showed that the MB sorption on the MSP adsorbent could not be described by any simple mechanism. It was a rather complex sorption process involving electrostatic interaction, multi-layer adsorption, several van der Waals interactions, and pore-filling.

The equilibrium sorption data at all temperatures studied were employed in calculating the thermodynamics parameters ( $\Delta H^\circ$ ,  $\Delta S^\circ$ , and  $\Delta G^\circ$ ) in Table 4. The  $\Delta G^\circ$  value indicates the spontaneity of the process; a negative value implies a spontaneous process, while a positive value implies a non-spontaneous one.<sup>48</sup> The negative  $\Delta G^\circ$  values for this study (Table 4) indicate that MB sorption on the MSP was spontaneous and thermodynamically feasible. The  $\Delta S^\circ$  value was positive, indicating a higher degree of freedom of the MB molecules remaining in solution as the sorption process proceeded toward equilibrium.<sup>4</sup> The  $\Delta H^\circ$  value obtained for this study was positive, implying that the experimental MB sorption process was endothermic;<sup>4,48</sup> thus, higher temperature should enhance the sorption process. This was not obvious in the experimental results, especially in Fig. 3a, but the data suggest that temperature may have little or no impact on the sorption of MB on the MSP adsorbent.

Table 4 Methylene blue sorption thermodynamic parameters

$\Delta H^\circ$ (kJ mol <sup>-1</sup> )	$\Delta S^\circ$ (J mol <sup>-1</sup> K <sup>-1</sup> )	$\Delta G^\circ$ (kJ mol <sup>-1</sup> )		
		288 K	298 K	308 K
59.35	207.60	-7.70	-2.90	-0.40

Table 5 Comparison of some reported biomass-based MB adsorbents

Adsorbent	$q_e$ (mg g <sup>-1</sup> )	Reference
Tamarind fruit shell	1.7	22
SPP	2.4	This study
Bone charcoal	5.0	49
Algal biomass	6.0	50
Defatted algal biomass	7.7	50
Acid-treated algal biomass	7.8	50
Sugar extracted spent rice biomass	8.1	51
Coir dust-activated carbon	14.3	52
MSP	14.3	This study
Sunflower oil cake activated carbon	16.4	53
Date seed biochar	42.5	54
Acid-treated cocoa nutshell	50.6	55
Raw pine cone biomass	109.9	56

The MSP composite reusability study was carried out for MB sorption over 5 cycles under identical experimental conditions as the pristine MSP adsorbent but after washing the used adsorbent with ethanol:water solution. The results are presented in Fig. 3c and it shows that MSP exhibited a sustained sorption efficiency of  $\approx 70\%$  even after 5 cycles of reuse. The loss of sorption capacity after each cycle did not exceed 9%, indicating gradual, rather than rapid, loss of capacity. These data suggest that the MSP composite is renewable and may be a viable option in water treatment.

To assess the relative efficiency of the MSP adsorbent to some other biomass-based adsorbents reported in the literature, a comparison was made as shown in Table 5. It was observed that the MSP composite exhibited  $\approx 500\%$  enhanced efficiency in comparison to the pristine SPP and was also better than several other reported adsorbents. Notwithstanding the enhanced sorption capacity, the ease of separation of the MSP adsorbent from water post-adsorption, its stability, and reusability are the major merits of this adsorbent over those reported in the literature.

## 4 Conclusion

Sweet potato peel (SPP) waste was valorized for contaminated water treatment by magnetizing the defatted peel waste (MSP) and employing MSP for methylene blue sorption from contaminated water. Sorption equilibrium was fast (20 min), and the adsorbent was effective over a wide pH (3–9) and temperature range (15–35 °C). Compared to the pristine SPP, the MSP exhibited enhanced cation exchange capacity (11%) and MB sorption potential ( $\approx 500\%$ ). The observed sorption capacity of the MSP for MB was 14.3 mg g<sup>-1</sup> and this is better than those of most biomass-based adsorbents reported in the literature. The composite exhibited good reusability with  $\approx 70\%$  efficiency after 5 cycles. The MB sorption mechanism was a rather complex process involving electrostatic interaction, multi-layer adsorption, several van der Waals interactions, and pore-filling. Notwithstanding the enhanced sorption capacity, the ease of magnetic separation of the MSP adsorbent from water post-adsorption, its stability, and reusability are the major merits of this adsorbent.



## Conflicts of interest

The authors have no relevant financial or non-financial interests to disclose.

## Acknowledgements

We acknowledge the Department of Chemical Sciences and Department of Environmental Management & Toxicology, University of Delta Agbor for their support.

## References

- 1 A. N. Ebelegi, N. Ayawei, D. Wankasi, E. D. Dikio, P. N. Diagboya and F. M. Mtunzi, *J. Environ. Chem. Eng.*, 2019, **7**, 103214.
- 2 P. N. E. Diagboya and E. D. Dikio, *Microporous Mesoporous Mater.*, 2018, **266**, 252–267.
- 3 P. R. Sera, P. N. Diagboya, S. O. Akpotu, F. M. Mtunzi and T. B. Chokwe, *Bioresour. Technol. Rep.*, 2022, **16**, 100881.
- 4 R. P. Mohubedu, P. N. E. Diagboya, C. Y. Abasi, E. D. Dikio and F. Mtunzi, *J. Cleaner Prod.*, 2019, **209**, 1016–1024.
- 5 P. N. Diagboya, B. I. Olu-Owolabi, D. Zhou and B.-H. Han, *Carbon*, 2014, **79**, 174–182.
- 6 P. N. Diagboya and E. D. Dikio, *J. Cleaner Prod.*, 2018, **180**, 71–80.
- 7 E. B. AttahDaniel, E. D. Dikio, N. Ayawei, D. Wankasi, F. M. Mtunzi and P. N. Diagboya, *Proc. Inst. Mech. Eng., Part N*, 2023, DOI: [10.1177/23977914231195748](https://doi.org/10.1177/23977914231195748).
- 8 P. N. Diagboya, B. I. Olu-Owolabi, F. M. Mtunzi and K. O. Adebawale, *Surf. Interfaces*, 2020, **19**, 100506.
- 9 H. K. Okoro, S. M. Alao, S. Pandey, I. Jimoh, K. A. Basheeru, Z. Caliphs and J. C. Ngila, *Appl. Water Sci.*, 2022, **12**, 259.
- 10 S. Pandey, N. Son, S. Kim, D. Balakrishnan and M. Kang, *Environ. Res.*, 2022, **214**, 114000.
- 11 P. N. Diagboya, J. Junck, S. O. Akpotu and R.-A. Düring, *Environ. Sci.: Processes Impacts*, 2024, DOI: [10.1039/D3EM000425B](https://doi.org/10.1039/D3EM000425B).
- 12 S. Pandey, S. Kim, Y. S. Kim, D. Kumar and M. Kang, *Environ. Res.*, 2024, **240**, 117540.
- 13 S. Pandey, E. Makhado, S. Kim and M. Kang, *Environ. Res.*, 2023, **217**, 114909.
- 14 P. N. Diagboya and E. D. Dikio, *Environ. Technol. Innovation*, 2018, **9**, 275–284.
- 15 B. I. Olu-Owolabi, A. H. Alabi, P. N. Diagboya, E. I. Unuabonah and R. A. Düring, *J. Environ. Manage.*, 2017, **192**, 94–99.
- 16 B. I. Olu-Owolabi, P. N. Diagboya and W. C. Ebaddan, *Chem. Eng. J.*, 2012, **195–196**, 270–275.
- 17 A. P. Meneghel, A. C. Gonçalves, F. Rubio, D. C. Dragunski, C. A. Lindino and L. Strey, *Water, Air, Soil Pollut.*, 2013, **224**, 1383.
- 18 E. D. Asuquo and A. D. Martin, *J. Environ. Chem. Eng.*, 2016, **4**, 4207–4228.
- 19 K. G. Akpomie and J. Conradie, *Environ. Chem. Lett.*, 2020, **18**, 1085–1112.
- 20 M. O. Omorogie, J. O. Babalola, E. I. Unuabonah and J. R. Gong, *Bioresour. Technol.*, 2012, **118**, 576–579.
- 21 K. G. Akpomie, A. C. Ofomatah, H. O. Chukwuemeka-Okorie, J. U. Ani, S. C. Agbo, O. A. Odewole, F. K. Ojo, O. L. Alum and J. Conradie, Equilibrium isotherm investigation on the sequestration of ciprofloxacin from solution via adsorption onto yam peel powder, *IOP Conference Series: Earth and Environmental Science*, 2023, vol. 1178, pp. 012020.
- 22 P. Saha, *Water, Air, Soil Pollut.*, 2010, **213**, 287–299.
- 23 M. P. Mudugamuwa Arachchige, T. Mu and M. Ma, *Chemosphere*, 2021, **262**, 128102.
- 24 W. Zhang, Y. Zhao, Q. Liao, Z. Li, D. Jue and J. Tang, *Molecules*, 2023, **28**, 819.
- 25 P. N. Diagboya, B. I. Olu-Owolabi and K. O. Adebawale, *RSC Adv.*, 2015, **5**, 2536–2542.
- 26 Z. P. Zanele, F. M. Mtunzi, S. M. Nelana, A. N. Ebelegi, N. Ayawei, E. D. Dikio, D. Wankasi and P. N. Diagboya, *Langmuir: the ACS J. Colloids Surf.*, 2021, **37**, 9764–9773.
- 27 B. I. Olu-Owolabi, A. H. Alabi, E. I. Unuabonah, P. N. Diagboya, L. Böhm and R.-A. Düring, *J. Environ. Chem. Eng.*, 2016, **4**, 1376–1382.
- 28 S. Lagergren, *Handlingar*, 1898, **24**, 1–39.
- 29 P. N. Diagboya, B. J. Heyde and R.-A. Düring, *Chem. Eng. J.*, 2023, 143263, DOI: [10.1016/j.cej.2023.143263](https://doi.org/10.1016/j.cej.2023.143263).
- 30 S. O. Akpotu, I. A. Lawal, P. N. Diagboya, F. M. Mtunzi and A. E. Ofomaja, *ACS Omega*, 2022, **7**, 34054–34065.
- 31 E. B. AttahDaniel, F. M. Mtunzi, D. Wankasi, N. Ayawei, E. D. Dikio and P. N. Diagboya, *Water, Air, Soil Pollut.*, 2022, **233**, 442.
- 32 C. P. Okoli, P. N. Diagboya, I. O. Anigbogu, B. I. Olu-Owolabi and K. O. Adebawale, *Environ. Earth Sci.*, 2017, **76**, 33.
- 33 E. D. Asuquo and A. D. Martin, *J. Environ. Chem. Eng.*, 2016, **4**, 4207–4228.
- 34 B. Chen, Z. Chen and S. Lv, *Bioresour. Technol.*, 2011, **102**, 716–723.
- 35 P. N. Diagboya, B. I. Olu-Owolabi and K. O. Adebawale, *RSC Adv.*, 2015, **5**, 2536–2542.
- 36 S. O. Akpotu, P. N. Diagboya, I. A. Lawal, S. O. Sanni, A. Pholosi, F. M. Mtunzi and A. E. Ofomaja, *Chem. Eng. J.*, 2023, **453**, 139771.
- 37 C. S. Castro, M. C. Guerreiro, M. Gonçalves, L. C. A. Oliveira and A. S. Anastácio, *J. Hazard. Mater.*, 2009, **164**, 609–614.
- 38 S. Darmawan, N. J. Wistara, G. Pari, A. Maddu and W. Syafii, *BioResources*, 2016, **11**, 3561–3574.
- 39 P. N. Diagboya and E. D. Dikio, *J. Cleaner Prod.*, 2018, **180**, 71–80.
- 40 M. Zhang, B. Gao, S. Varnoosfaderani, A. Hebard, Y. Yao and M. Inyang, *Bioresour. Technol.*, 2013, **130**, 457–462.
- 41 B. I. Olu-Owolabi, P. N. Diagboya, E. I. Unuabonah, A. H. Alabi, R.-A. Düring and K. O. Adebawale, *J. Cleaner Prod.*, 2018, **171**, 884–891.
- 42 B. I. Olu-Owolabi, P. N. Diagboya, F. M. Mtunzi, K. O. Adebawale and R.-A. Düring, *Gondwana Res.*, 2022, **105**, 311–319.
- 43 B. I. Olu-Owolabi, P. N. Diagboya and K. O. Adebawale, *J. Environ. Manage.*, 2014, **137**, 1–9.





- 44 B. I. Olu-Owolabi, P. N. Diagboya and K. O. Adebawale, *Geoderma*, 2015, **239–240**, 179–185.
- 45 P. N. Diagboya, F. M. Mtunzi, R.-A. Düring and B. I. Olu-Owolabi, *Ind. Eng. Chem. Res.*, 2021, **60**, 2365–2373.
- 46 P. N. Diagboya, F. M. Mtunzi, K. O. Adebawale, R.-A. Düring and B. I. Olu-Owolabi, *Colloids Surf., A*, 2021, 127930, DOI: [10.1016/j.colsurfa.2021.127930](https://doi.org/10.1016/j.colsurfa.2021.127930).
- 47 B. I. Olu-Owolabi, P. N. Diagboya, F. M. Mtunzi and R.-A. Düring, *J. Environ. Manage.*, 2021, **279**, 111619.
- 48 C. P. Okoli, G. O. Adewuyi, Q. Zhang, P. N. Diagboya and Q. Guo, *Carbohydr. Polym.*, 2014, **114**, 440–449.
- 49 G. Ghanizadeh and G. Asgari, *React. Kinet., Mech. Catal.*, 2010, **102**, 127–142.
- 50 T. Sarat Chandra, S. N. Mudliar, S. Vidyashankar, S. Mukherji, R. Sarada, K. Krishnamurthi and V. S. Chauhan, *Bioresour. Technol.*, 2015, **184**, 395–404.
- 51 M. S. U. Rehman, I. Kim and J.-I. Han, *Carbohydr. Polym.*, 2012, **90**, 1314–1322.
- 52 S. Macedo Jde, N. B. da Costa Junior, L. E. Almeida, E. F. Vieira, A. R. Cestari, F. Gimenez Ide, N. L. Villarreal Carreno and L. S. Barreto, *J. Colloid Interface Sci.*, 2006, **298**, 515–522.
- 53 S. Karagöz, T. Tay, S. Ucar and M. Erdem, *Bioresour. Technol.*, 2008, **99**, 6214–6222.
- 54 Z. Mahdi, A. E. Hanandeh and Q. Yu, *Waste Biomass Valorization*, 2017, **8**, 2061–2073.
- 55 A. H. Jawad, A. S. Abdulhameed and M. S. Mastuli, *J. Taibah Univ. Sci.*, 2020, **14**, 305–313.
- 56 T. K. Sen, S. Afroze and H. M. Ang, *Water, Air, Soil Pollut.*, 2011, **218**, 499–515.

